forests

MDPI

Article

Stem Circadian Phenology of Four Pine Species in Naturally Contrasting Climates from Sky-Island Forests of the Western USA

Emanuele Ziaco and Franco Biondi *

DendroLab, Department of Natural Resources and Environmental Science, University of Nevada, Reno, NV 89557, USA; eziaco@unr.edu

* Correspondence: fbiondi@unr.edu; Tel.: +1-775-784-6921

Received: 12 June 2018; Accepted: 29 June 2018; Published: 4 July 2018

Abstract: We identified intra-annual climatic drivers of stem water relationships and growth in foundation conifers at a subalpine site in the Great Basin Desert and at a montane site in the Mojave Desert (Nevada, USA). Sites were instrumented to represent naturally different levels of heat and drought stress as part of NevCAN (the Nevada Climate and ecohydrological Assessment Network). We analyzed three years (2013–2015) of sub-hourly dendrometer records for limber (*Pinus flexilis*) and bristlecone pine (*Pinus longaeva*) at the subalpine site, and for ponderosa (*Pinus ponderosa*) and pinyon pine (*Pinus monophylla*) at the montane site. Multiple logistic regression was used to identify relationships with environmental variables measured in-situ. At both sites, stem expansion occurred during the early morning and late afternoon, and irreversible stem increment was concentrated in the early morning hours. In subalpine species, stem growth started in late spring and continued until August, while at the montane site stem growth was episodic, peaking during summer monsoonal rainstorms. Circadian maximum and minimum stem size during the growing season were reversed during the dormant season at the colder/wetter subalpine site but not at the warmer/drier montane one. Knowledge of intra-annual tree-water relationships and stem growth helps understand how sky island forests grow under highly diverse climatic conditions, including severe drought and heat stress.

Keywords: arid environments; tree water deficit; point dendrometers; hydroclimate; north American monsoon; stem water dynamics; *Pinus longaeva*; *Pinus flexilis*; *Pinus ponderosa*; *Pinus monophylla*

1. Introduction

The functioning and health of forest ecosystems depend on the adaptation of dominant tree species to varying environmental conditions at multiple timescales [1]. Annual to multi-decadal climate-growth relationships have been investigated in a broad range of biomes for a number of conifer and broadleaf species using tree-ring proxies [2]. In order to understand how forest ecosystems will fare under future global warming scenarios, it has become increasingly important to investigate the physiological basis of individual plant adaptation to different levels of environmental stress [3–5]. Attention has therefore been driven towards identifying the mechanisms underlying patterns of hourly to sub-hourly stem growth [6,7] and in particular how such patterns are affected by meteorological and environmental variables under natural conditions [8,9].

Daily variations of woody stem size are the consequences of reversible phases of shrinkage and swelling, reflecting reversible dynamics of stem water storage, as well as irreversible stem growth [10]. Stem contraction occurs when water uptake from the soil does not compensate for water losses from canopy evapotranspiration [11], forcing the plant to recall water from the elastic tissues of the stem

(i.e., phloem, bark) into the sapwood [12]. Contrarily, when absorption from the roots is greater than the amount of water lost to the atmosphere, expansion of the stem is observed [13]. However, under hyperarid conditions a tree may undergo prolonged periods of stem shrinkage [14]. Recently an innovative methodological approach was proposed to separate water-deficit induced stem shrinkage from irreversible radial growth [15], assuming that no growth is occurring during stem shrinkage because of limited turgor pressure in the cambium cells [7].

The amount of water stored in tree stems and its contribution to daily water fluxes depends on the tree species and individual characteristics, in particular tree size [16]. Stems, especially the sapwood, hold the largest reserve of water in trees, and larger individuals hold greater reserves of water available to fulfill daily physiological processes [17]. Larger proportions of sapwood may also facilitate water movement through the stem under lower tensions compared to species with less sapwood under similar evapotranspiration demands [18]. Even if the proportion of sapwood over total basal area is not linked to environmental conditions [19], climatic stressors (such as drought) may deplete internal storage by increasing water demand for transpiration [20] or by preventing the replenishment of reserves [21].

Monitoring stem-radius changes using automated dendrometers is a widely used method to define stem water dynamics [11,20,22,23] and tree growth response to short-term climatic factors [24]. Daily oscillations define the stem circadian cycle, which is composed by a contraction phase (i.e., depletion of water reserves), an expansion phase (i.e., replenishment of water reserve), and occasionally a stem increment phase [22]. While diurnal (or diel) cycles depend on evapotranspiration, ultimately balancing root uptake with canopy losses under normal conditions [12], prolonged periods of stem swelling or shrinking may result in long cycles exceeding 24 h [4]. Positive/negative fluctuations of stem radius resulting from diurnal and long cycles can then be used to highlight correlations with environmental variables and their effect on tree growth and stem water dynamics ([10] and references therein).

The Great Basin and Mojave Deserts of the western USA are characterized by arid and semi-arid conditions, and water availability is generally the main limiting factor for natural systems [25]. Both deserts are characterized by pronounced elevation gradients in precipitation and temperature, so that mountain ranges, depending on their elevation and topography, can be dominated by sky-island conifer forests that experience dry and hot summers as well as cold and snowy winters [26]. Latitudinal variability in climate also exists, as the northern areas tend to be characterized by winter and spring precipitation, with associated snowpack dynamics, whereas the southern areas tend to be more affected by summertime rainfall brought by the northwest edge of the North American Monsoon system [27]. Tree species growing in these regions are able to survive under a climatic regime characterized by periods of hyperarid conditions [28], so that greater understanding of their ecohydrological dynamics may help predict how tree species will fare under the warmer and drier world forecasted by global warming scenarios in the western US.

We assessed tree-water relationships and the environmental drivers of stem circadian cycles in four "foundation" [29] conifer species from the Great Basin and Mojave deserts of North America. We analyzed three years (2013–2015) of continuous dendrometer records from two contrasting locations: a subalpine site in the central Great Basin and a montane site at the border between the Mojave and Great Basin deserts. Our study objectives were: i) to characterize daily and seasonal stem circadian cycles in conifers experiencing different levels of heat and drought stress; ii) to characterize seasonal dynamics and patterns of tree water deficit and irreversible radial growth; and iii) to investigate the climatic drivers of stem size variations in order to assess species-specific levels of adaptation to local conditions and hypothesize their responses to future warming scenarios.

2. Materials and Methods

2.1. Study Area

Two sites separated by 2.5° latitude were instrumented for this study as part of the Nevada Climate-ecohydrological Assessment Network (NevCAN; Figure 1a). Automated sensors were installed between 2010 and 2013 to measure climatic and environmental variables at sub-hourly time intervals [30]. The Snake Subalpine West site (38°54′22″ N, 114°18′32″ W; 3355 m a.s.l.) is located on the western flank of the Snake Range in central-eastern Nevada. Vegetation is a mixed-conifer stand dominated by bristlecone pine (*Pinus longaeva* D. K. Bailey), limber pine (*Pinus flexilis* E. James), and Engelmann spruce (*Picea engelmannii* Parry ex Engelm.). The Sheep Montane site (36°35′25″ N, 115°12′51″ W; 2320 m a.s.l.) is located in southern Nevada, about 50 km north of Las Vegas. The canopy is composed of ponderosa pines (*Pinus ponderosa* var. *scopulorum* Engelm.) and pinyon pines (*Pinus monophylla* Torr. & Frém.). The shrub layer is absent or extremely sporadic at both sites. Parent rock material at both sites is composed by a colluvium derived from limestone and dolomite. Soils are loamy-skeletal Lithic Cryorthens at the Snake Range location, and loamy-skeletal Aridic Lithic Haplustolls at the Sheep Range site [31].

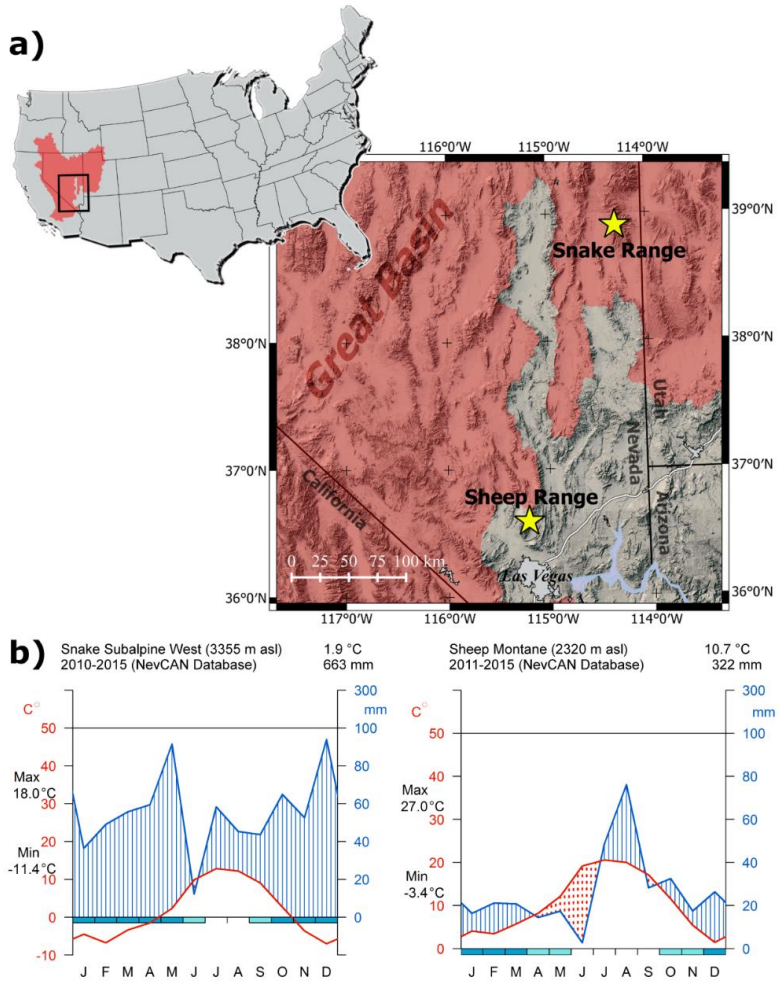

Figure 1. (**a**) Geographic location of the two study sites with respect to the hydrographic boundary of the Great Basin (red shaded area). (**b**) Walter-Lieth climatic diagrams for the two study sites with temperature (red labels) on the left y axis and total precipitation (blue labels) on the right one. Bars below the x-axes indicate frost season (dark blue), probable frost season (light blue), and frost-free season (no bars).

The Snake Range, which falls within the hydrographic Great Basin, is characterized by cool-season precipitation and associated winter snowpack dynamics. Average annual temperature during the first five years of NevCAN operation (2010–2015) was 1.9 °C, and average total annual precipitation was 663 mm (Figure 1b). The Sheep Range is located near the hydrographic boundary between the Great Basin and the Mojave Desert, one of the driest regions influenced by the North American Monsoon [32]. Based on NevCAN data for 2011–2015, the mean annual temperature was 10.7 °C, and the mean total annual precipitation was 322 mm, mostly concentrated in July and August (Figure 1b).

2.2. Dendrometer Data

Automated point dendrometers manufactured by Agricultural Electronics Corporation (Tucson, Arizona, USA) were installed on two pine species at each of the two sites. Observational noise caused by the hydration and de-hydration of the bark is minimized by the mm^2-area of the sensor tip and by shaving off the outer bark before installing the sensor [33]. Stem radius is quantified by measuring the horizontal linear displacement of a sensing rod, which is then turned into an electric signal with a resolution of 4 μm over a range of 15,000 μm [34]. At the Snake Range, a total of 12 dendrometers were installed on 6 bristlecone pines (*Pinus longaeva*, abbreviated as PILO), and 7 dendrometers were installed on 4 limber pines (*Pinus flexilis*, PIFL) (on one tree it was possible to install only one dendrometer). At the Sheep Range, a total of 8 dendrometers were installed on 4 ponderosa pines (*Pinus ponderosa*, PIPO) and 8 dendrometers were installed on 4 pinyon pines (*Pinus monophylla*, PIMO). Trees equipped with two dendrometers at different height along the stem, usually between the ground level and about 1.5 m, were used to test that dendrometer traces did not depend on sensor location. For each species, there was at least one dendrometer located in one of the four cardinal directions.

Instrumented trees were selected to represent the variability of stem sizes under natural conditions. At the Snake Range the average diameter of instrumented trees was 41 ± 15 cm for PILO and 21 ± 9 cm for PIFL, and the average height was 8 ± 2 m and 5 ± 2 m, respectively. Average diameter at the Sheep Range was 53 ± 8 cm for ponderosa pine (mean height = 11 ± 2 m) and 30 ± 7 cm for pinyon pine (mean height = 6 ± 2 m). Bristlecone pines instrumented at the Snake Range exceeded 240 years of age [35], even though one of them was large enough that its stem age exceeded multiple centuries, while limber pines usually did not exceed 100 years of age [14]. At the Sheep Range, age of instrumented ponderosa and pinyon pines reached a maximum greater than 250 years.

2.3. Climatic Data

Climatic data recorded by the NevCAN stations were obtained from the Western Regional Climate Center (www.wrcc.dri.edu/SRtransect/; www.wrcc.dri.edu/GBtransect/) and used to produce hourly summaries for atmospheric and soil variables [35]. Correlation analysis was used to assess the degree of predictor multicollinearity, and seven variables were selected for further study (Table 1): mean air temperature (AirT), mean soil temperature at 50 cm belowground (SoilT), soil volumetric water content at 17 cm (VWC_{17}) and 32 cm (VWC_{32}), total precipitation (PPT), dew point (Dew), and Vapor Pressure Deficit (VPD). Dew point is directly related to atmospheric moisture content [36] and its importance in hydrologic modeling is well recognized in the western US [37,38]. Dew point synthetizes four atmospheric variables (relative humidity, barometric pressure, saturated and ambient vapor pressure), which are required for its computation. Relative humidity (%) and barometric pressure (mb) were acquired from the NevCAN station, while vapor pressures (hPa) were computed according to standard formulas (equations (1) and (2), [34]) and then used to calculate dew point (°C; equation (A.4) [39]).

Table 1. Summary of climatic variables included in this study. Hourly means and range (minimum/maximum) are shown for the June-September period during 2013–2015 (average climate conditions for the whole year are shown in Figure 1b).

Variable	Code	Unit	Snake Range Subalpine West	Sheep Range Montane
Air temperature	AirT	°C	10.4 (−12.8/25.7)	18.8 (−5.8/36.6)
Soil temperature (50 cm)	SoilT	°C	13.7 (−0.6/21.4)	19.0 (8.6/23.6)
Soil volumetric water content (17 cm)	VWC_{17}	%	7.0 (2.4/22.1)	6.9 (4.4/13.9)
Soil volumetric water content (32 cm)	VWC_{32}	%	8.8 (4.1/18.4)	8.3 (6.6/10.2)
Dew point	Dew	°C	−2.6 (−34.6/8.9)	0.7 (−25.1/17.0)
Vapor Pressure Deficit	VPD	hPa	7.7 (0.2/21.7)	15.5 (0.2/42.2)
Total precipitation	PPT	mm	179 (0/9)	171 (0/51)

2.4. Extraction of Stem-Cycle Phases

All dendrometer records were processed using *dendrometeR* [40], a task-specific, open-source, statistical package for analyzing sub-daily dendrometer data within the R software environment [41]. Half-hourly individual dendrometer measurements from January 1st 2013 to December 31st 2015 were converted into daily stem increments by subtracting the previous day maximum from the current day maximum, and then transformed into cumulative series by adding daily stem increments. Quality control was performed to identify data gaps due to malfunctioning of dendrometers or data loggers. Graphical and numerical data summaries were used to detect errors, and values > ± 2 standard deviations from the daily mean were set as missing. No data gaps >12 h were found in our records, and any shorter gaps were filled using an ARIMA model, as it is typically done in these studies [42]. To enhance the signal-to-noise ratio at the stand level while reducing possible effects of tree size on individual measurements, corrected half-hourly records were combined in a site composite by species [23]. Daily and monthly mean circadian cycles were computed for each species by aggregating half-hourly measurements of stem radius from 2013 to 2015.

Xylogenesis studies conducted through repeated microcoring at the Snake Range on both *P. longaeva* [35] and *P. flexilis* [14] found that the production of new xylem cells begins in early June and continues until the end of August. At the Sheep Range, cellular measurements conducted on *P. ponderosa* in 2015 and 2016 have shown that cambial phenology is driven by moisture availability, with the formation of new tracheids occurring earlier in the spring after wet winters, but delayed to late June-early July when water is supplied through monsoonal precipitation [43]. Therefore we included in our analysis circadian cycles that started after June 1st and ended before September 30th.

Since daily cycles of stem size variations do not cover exactly a 24-h period [23], we distinguished diurnal cycles (duration <28 h) from long cycles (duration ≥28 h) [4]. Long cycles from June to September exceeded the average duration of diurnal cycles by two standard deviations or more. For each species, we identified three different phases in circadian cycles [22]: 1) contraction (i.e., period between a maximum in stem radius and the following minimum); 2) expansion (i.e., period between a daily minimum and the following maximum); 3) stem increment (i.e., that portion of the expansion phase starting when stem radius exceeds the previous cycle's maximum). For each phase and for each whole cycle, defined as contraction + expansion + increment (when present), we computed the onset (hour of the day), the duration (hours) and the magnitude (µm), i.e., the difference between maximum and minimum stem radius.

2.5. Modeling Relationships between Climate, Tree Water Deficit (TWD), and Real Growth (RG)

Stem water dynamics were analyzed separately from irreversible stem radial growth for each species. To investigate daily patterns of stem water depletion and replenishment, we pooled together expansion and increment phases to indicate "stem swelling" (SS), which indicates recharging stem water reserves. Stem increment phases (*sensu* [22]) are often not associated with a "real"

radial increment, especially when they occur as isolated peaks during prolonged phases of stem shrinkage [44]. Therefore, to identify radial growth causing an actual increment in stem diameter, we first created hourly time series of tree water deficit (TWD) according to [15]. Briefly, TWD is a measure of stem shrinkage caused by water deficit, and it is measured in the same unit as stem radius (either µm or mm). TWD is usually <0, indicating that the current stem radius is below the previous highest recorded radius. When TWD equals 0, stem radius is increasing, stem water potential is near saturation, and therefore irreversible real growth (RG) is observed [15]. Hourly values of stem radius measured at TWD = 0 were used to compute curves of cumulative RG from June 1st to September 30th.

Because dendrometers readings can be affected by tree size, we used a probabilistic approach to assess how the presence/absence of circadian phases, rather than their magnitude, was controlled by climatic drivers. The relationship between environmental variables, stem swelling/shrinkage, and real growth was investigated by species and for different time lags using logistic regression. Summaries for each climatic variable were calculated up to a 24-h lag with a 3-h interval (i.e., t_0, t_{-3}, t_{-6}, ... , t_{-24}), producing a total of nine time lags for each explanatory variable (i.e., AirT, PPT, SoilT, VWC_{17}, VWC_{32}, VPD and Dew), and a total of 63 predictors. Each hourly observation of stem size was converted to a binomial variable, with "0" for shrinkage and "1" for swelling. Analogously, each hourly record was converted to a binomial variable depending on the presence/absence of RG, with "1" for growth and "0" for no growth. A blockwise variable selection was performed to select within each group of variables the time lag that best fitted the binary dataset of stem swelling and real growth using simple logistic regression:

$$Logit\ (\pi_x)\ln\left(\frac{\pi_x}{1-\pi_x}\right) = \beta_0 + \beta_1 x$$

with π_x being the probability of stem swelling (or real growth) for a given value of climatic parameter x, and β_0 and β_1 the intercept and slope of the regression. Goodness of fit for each model was assessed using a Hosmer-Lemeshow test [45], and significance of individual parameters was tested with Wald's χ^2 [46]. If two or more variables, at any time lag, passed the Hosmer-Lemeshow test, then those variables were combined into a multiple logistic regression [45]:

$$Logit\ (\pi_x) = \ln\left(\frac{\pi_x}{1-\pi_x}\right) = \beta_0 + \beta_1 x + \beta_2 y + \ldots + \beta_n z$$

where x, y, and z are the n selected climatic variables, β_0 the intercept of the regression, and β_1, β_2, and βn the coefficients for the n climatic variables. The Hosmer-Lemeshow test was used again to evaluate model calibration, while model discrimination capacity (i.e., the model's ability to predict an event correctly) was assessed measuring the area under a Receiver Operating Characteristic (ROC) curve [47] computed using the R package *pROC* [48]. In order to account for time-of-day influence on stomatal conductance and xylem water potentials, models of stem swelling and real growth were computed separately for night (19:00–6:00) and day hours (7:00–18:00). Since more than 90% of the seasonal cumulative real growth was completed by the end of August, the relationship between climate, TWD, and RG was analyzed for the June-August period.

3. Results

3.1. Climate

Climatic data from 2013 to 2015 highlight differences between the two study sites (Figure 2), in particular for seasonal dynamics of precipitation and soil temperature. Average air and soil temperature during the summer at the Sheep Range site were higher, respectively by 8.4 °C and 5.3 °C, than at the Snake Range site (Table 1). At the Sheep Range, soil temperature at 50-cm depth was close to 0 °C only occasionally between December and January (Figure 2), while at the Snake Range soil temperature at 50-cm depth was constantly near 0 °C from November to May because of snowpack presence. From June to August, daily variability of soil temperature was higher at the Snake Range

(northern site) than at the Sheep Range (southern site) because of larger thermal excursion between night and day. The average volumetric water content of both shallow (VWC_{17}) and deep (VWC_{32}) soil was similar at the two sites, despite a much broader range of soil moisture from June to August at the Snake Range (Table 1).

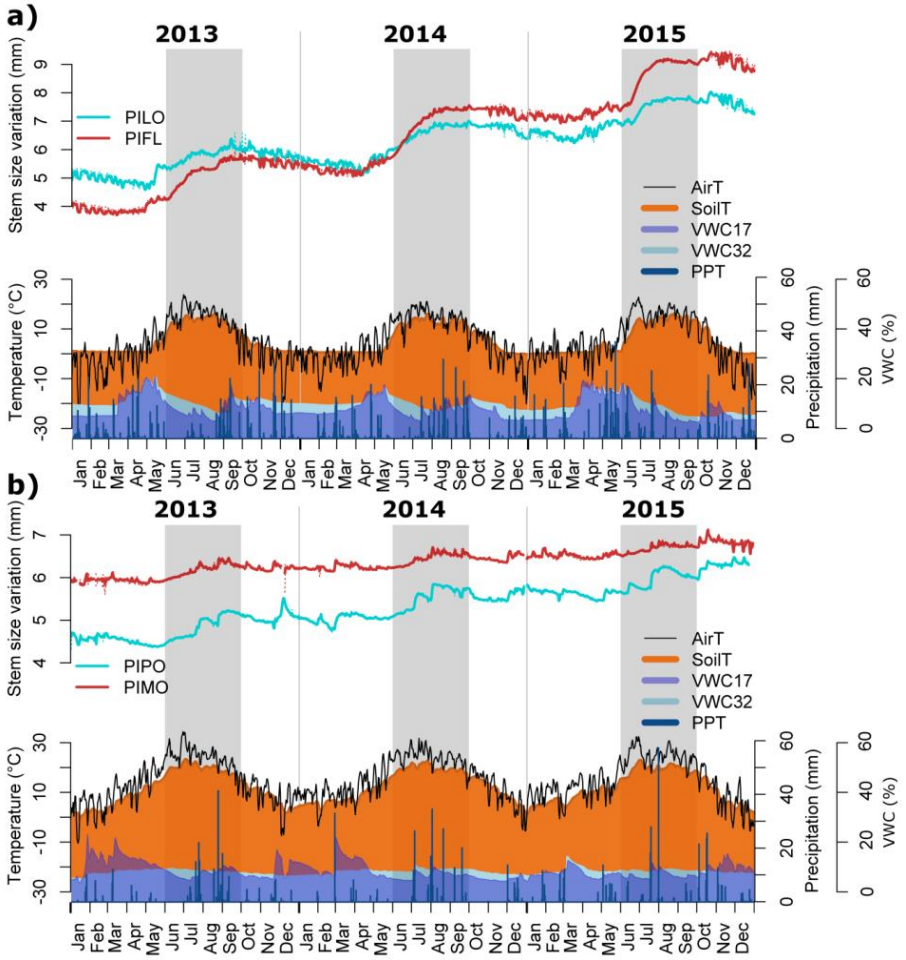

Figure 2. Site-wide composites of stem size variation during 2013–2015 computed for: (**a**) *Pinus longaeva* (PILO) and *Pinus flexilis* (PIFL) at the Snake Range Subalpine West site and (**b**) for *Pinus ponderosa* (PIPO) and *Pinus monophylla* (PIMO) at the Sheep Range Montane site. Daily time series of mean air temperature (AirT), soil temperature at 50 cm belowground (SoilT), volumetric water content at 2–17 cm (VWC_{17}) and 17–21 cm belowground (VWC_{32}), and total precipitation (PPT) are also shown. Gray shaded areas represent the 4-month period (June–September) considered for the analysis of circadian stem size phenology.

At both sites, no significant correlation emerged between VWC_{17} and VWC_{32} within a time lag of ±3–4 days. Total June–September precipitation was similar between the two sites (Table 1), even though at the Sheep Range precipitation was mostly concentrated in the July–August period. In fact, during 2013–2015 the fraction of total annual precipitation falling in July–August was only 15% at the Snake Range, but about 41% at the Sheep Range because of the North American Monsoon system. Consequently, during June–September average dew point was higher at the Sheep Range (0.7 °C) than at the Snake Range (−2.6 °C), even though the average vapor pressure deficit during the same period was almost twice as large at the Sheep Range than at the Snake Range (Table 1).

3.2. Seasonal and Daily Dynamics of Stem-Size Variation

Dendrometer traces (Figure 2) recorded at the Snake Range on PILO and PIFL (the northern species) displayed stem increment starting in May–June, concurrent with increasing deep soil temperature, and lasting until the end of August, with a subsequent gradual shrinkage during the winter (Figure 2a). At the Sheep Range, stem-size variation for both PIPO and PIMO (the southern species) was smaller, with major stem enlargement occurring in July with the arrival of monsoonal precipitation (Figure 2b). On average, stem-radius increase was 3.1 ± 1.1 mm for PILO and 5.2 ± 1.3 mm for PIFL between June 1st 2013 and September 30th 2015 (Figure 3a,b), while in the same period PIPO and PIMO showed lower size increases, respectively 2.2 ± 0.7 mm and 1.4 ± 0.6 mm (Figure 3c,d).

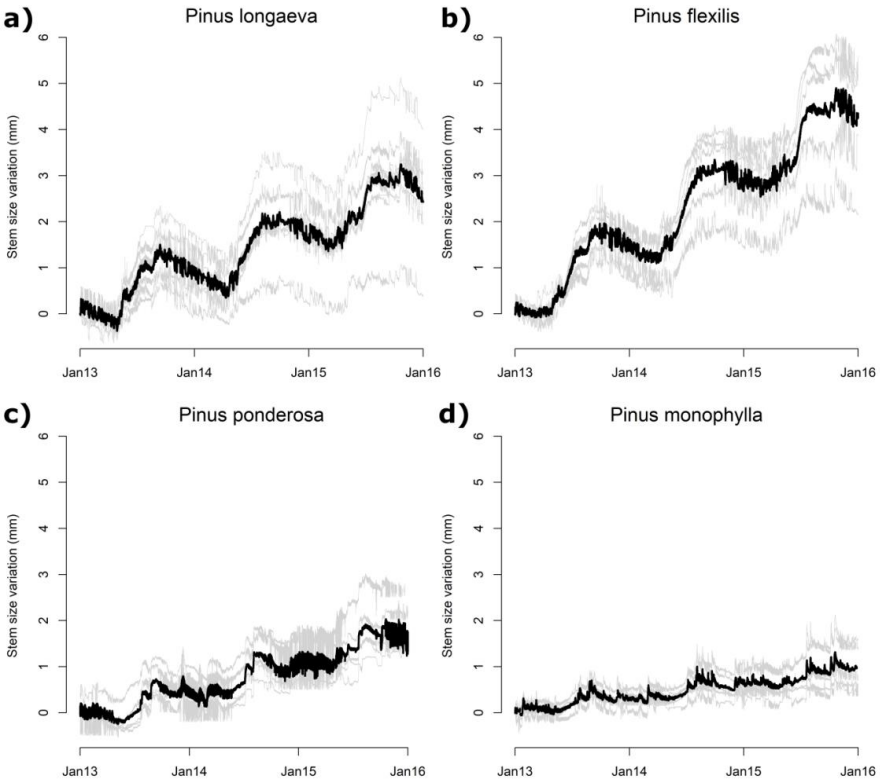

Figure 3. Half-hourly individual dendrometer tracks of stem size variation (gray lines) for PILO (**a**), PIFL (**b**), PIPO (**c**), and PIMO (**d**) from 1 January 2013 to 31 December 2015. Black bold lines represent the site average. Species codes are the same as in the Figure 2 caption.

Circadian cycles showed seasonal variability and substantial differences between the northern and southern pine species. At the Snake Range circadian cycles occurring during the cold season (November–May) were opposite in phase than those occurring during the warm season and the early fall (June–October) (Figure 4a). During the winter, for both PILO and PIFL, minimum stem radius occurred in the morning (7:00–7:30), while maxima were in the afternoon (15:30–16:00). During the summer and the early autumn, stem radius reached the maximum in the first hours of the morning in PILO (5:30) and a couple of hours later in PIFL (8:00). Then daily shrinkage began, culminating in the afternoon, first in PIFL (15:30) and then in PILO (17:00). At the Sheep Range no differences emerged between cold- and warm-season stem cycles in PIPO and PIMO (Figure 4b). Maximum stem radius occurred during the morning, first in PIMO (6:30–7:30) and then in PIPO (8:00–8:30). Minimum radial dimension was observed in the afternoon (16:30–17:00) during the warmest months, and about two hours later (18:00–18:30) during the cold season.

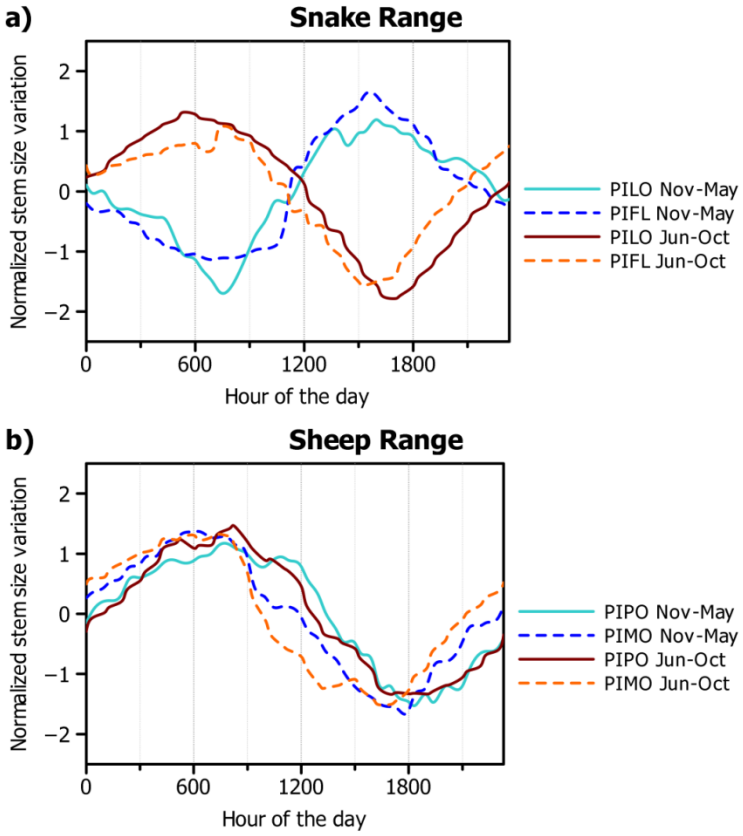

Figure 4. Daily circadian cycles calculated over three consecutive years (from January 2013 to December 2015) and averaged by species for the winter/spring (November–May) and for the summer/early autumn (June–October) at (**a**) the Snake Range, and (**b**) the Sheep Range. Species codes are the same as in the Figure 2 caption.

The average number of full cycles completed between June 1st and September 30th during the three years of study was 99 for PILO and 105 for PIFL at the Snake Range, and slightly less at the Sheep Range for PIPO (87) and PIMO (97). PIMO showed the highest amount of long cycles (60, representing 21% of total cycles), while in PIFL only 16% of all cycles were long (49). The duration of diurnal cycles was similar between species and sites, ranging between 23.7 and 23.8 hours (Table 2).

The onset of contraction started earlier at the Snake Range (05:20 in PILO and 04:29 in PIFL) than at the Sheep Range (06:49 in PIPO and 05:40 in PIMO). On average each diurnal cycle caused a positive increment of stem radius, as the stem size increase caused by the replenishment of stem water reserves (i.e., swelling) was larger than the reduction associated with water depletion (i.e., shrinkage). Average daily stem increment was about 1 µm for PIMO and 6 µm for PIPO at the Sheep Range, while it was about 4 µm in PILO and 11 µm in PIFL at the Snake Range. Long cycles, which showed very high variability, were longer at the Sheep Range (57.7 h in PIPO and 52.3 h in PIMO) compared to the Snake Range (52.1 h in PILO and 46.1 h in PIFL), but lower in magnitude (Table 2). The average increment of stem radius associated to long cycles was highest in PIPO (65 µm), and lowest in PIMO (38 µm).

Stem increment phases were mainly associated with long cycles: on average 68% of long cycles showed a stem increment phase against 48% of diurnal cycles, without any site-related difference between species. Long cycles produced higher stem increments, reflected in magnitudes that were three–four times larger than in diurnal cycles (Table 2). The duration of each phase was directly linked to its magnitude in all species, in particular for the increment, with similar correlations for PILO (Pearson's correlation coefficient $r = 0.89$, $p < 0.001$), PIFL ($r = 0.80$, $p < 0.001$) and PIPO ($r = 0.89$, $p < 0.001$) but lower in PIMO ($r = 0.68$, $p < 0.001$) (Figure S1).

Table 2. Summary statistics (mean ± 1 standard deviation) by species and phase at our study sites for diurnal and long cycles of stem variation occurring from June to September (see text for details). Onset = hour of day; Duration = hours; Magnitude = µm.

			Snake Range		Sheep Range	
Phase	**Type**	**Feature**	***Pinus longaeva***	***Pinus flexilis***	***Pinus ponderosa***	***Pinus monophylla***
Contraction	Diurnal	Onset	5:20 ± 1 h 51 m	4:29 ± 1 h 31 m	6:46 ± 2 h 16 m	5:40 ± 1 h 51 m
		Duration	11.3 ± 2.0	9.9 ± 1.6	10.8 ± 2.5	9.6 ± 2.2
		Magnitude	85 ± 40	69 ± 28	35 ± 50	60 ± 44
Expansion	Diurnal	Onset	16:16 ± 1 h 36 m	14:11 ± 1 h 33 m	17:05 ± 2 h 23 m	15:14 ± 1 h 30 m
		Duration	10.6 ± 2.3	10.2 ± 3.6	11.6 ± 3.0	12.6 ± 3.2
		Magnitude	75 ± 39	59 ± 27	28 ± 13	48 ± 24
Increment	Diurnal	Onset	4:52 ± 7 h 22 m	13:39 ± 9 h 01 m	5:19 ± 5 h 07 m	7:38 ±7 h 30 m
		Duration	3.5 ± 2.1	6.0 ± 3.4	3.1 ± 2.4	4.5 ± 4.4
		Magnitude	14 ± 14	21 ± 18	13 ± 73	13 ± 22
Whole cycle	Diurnal	Onset	5:20 ± 1 h 51 m	4:29 ± 1 h 31 m	6:46 ± 2 h 16 m	5:40 ± 1 h 51 m
		Duration	23.7 ± 1.9	23.8 ± 1.6	23.7 ± 1.9	23.8 ± 1.7
		Magnitude	95 ± 43	87 ± 27	44 ± 69	72 ± 61
Contraction	Long	Onset	6:58 ± 4 h 59 m	5:34 ± 4 h 40 m	7:39 ± 3 h 26 m	7:07 ± 4 h 41 m
		Duration	22.6 ± 14.3	14.9 ± 8.3	21.8 ± 19.2	19.8 ± 21.6
		Magnitude	73 ± 69	61 ± 38	35 ± 24	48 ± 34
Expansion	Long	Onset	15:25 ± 3 h 08 m	14:26 ± 1 h 59 m	17:42 ± 2 h 45 m	15:33 ± 1 h 47 m
		Duration	14.2 ± 11.6	15.3 ± 9.9	21.1 ± 19.4	23.7 ± 16.1
		Magnitude	45 ± 36	51 ± 34	30 ± 18	39 ± 29
Increment	Long	Onset	9:09 ± 7 h 04 m	12:33 ± 7 h 55 m	11:14 ± 8 h 05 m	11:58 ± 6 h 52 m
		Duration	24.4 ± 17.8	19.5 ± 14.0	25.4 ± 27.6	15.8 ± 15.6
		Magnitude	71 ± 54	53 ± 44	70 ± 101	47 ± 56
Whole cycle	Long	Onset	7:05 ± 4 h 57 m	5:24 ± 4 h 33 m	7:43 ± 3 h 26 m	7:10 ± 4 h 43 m
		Duration	52.1 ± 23.5	46.1 ± 16.6	57.7 ± 32.3	52.3 ± 27.8
		Magnitude	122 ± 90	111 ± 56	84 ± 94	85 ± 63

3.3. Climatic Influences on Tree Water Deficit and Real Growth

Time series of tree water deficit (TWD) showed different seasonal patterns of stem shrinkage/swelling between the Snake (Figure 5) and the Sheep Range (Figure 6). In general, all species experienced periods of water stress, particularly in the second part of the growing season (i.e., August). PILO and PIFL experienced lower values of TWD compared to PIPO and PIMO during June and part of July. At the Snake Range TWD values reached zero almost every day, at least for a few hours, resulting in a slow but constant real growth. A similar pattern was observed at the Sheep Range in June 2013 and 2014, but not later in the growing season, when TWD dropped for both PIPO and PIMO to approximately −0.25 mm, and RG occurred as episodic pulses driven by the onset of monsoonal precipitation (Figure 6). In 2015, after a severely dry winter, real growth for both species at the monsoonal site was concentrated in just three pulses during three major rainstorms: first in mid-June, second in mid-July, and third in early August. At the Snake Range, the species characterized by smaller individuals (PIFL) completed 25%, 50%, and 75% of total June–September radial increment usually 1–2 weeks before the species with larger average stems (PILO). At the Sheep Range radial growth was simultaneous between the two species, with no size effect. Stem swelling between June 1st and September 30th occurred prevalently during the night, between 18:00 and 06:00, especially at the Snake Range, whereas at the Sheep Range stem swelling was observed until 08:00 (Figure 7a,b). Real growth took place only in the morning hours, between 02:00 and 08:00 at the Sheep Range (with a drop between 06:00 and 07:00; Figure 7c) and between 04:00 and 05:00 at the Snake Range (Figure 7d).

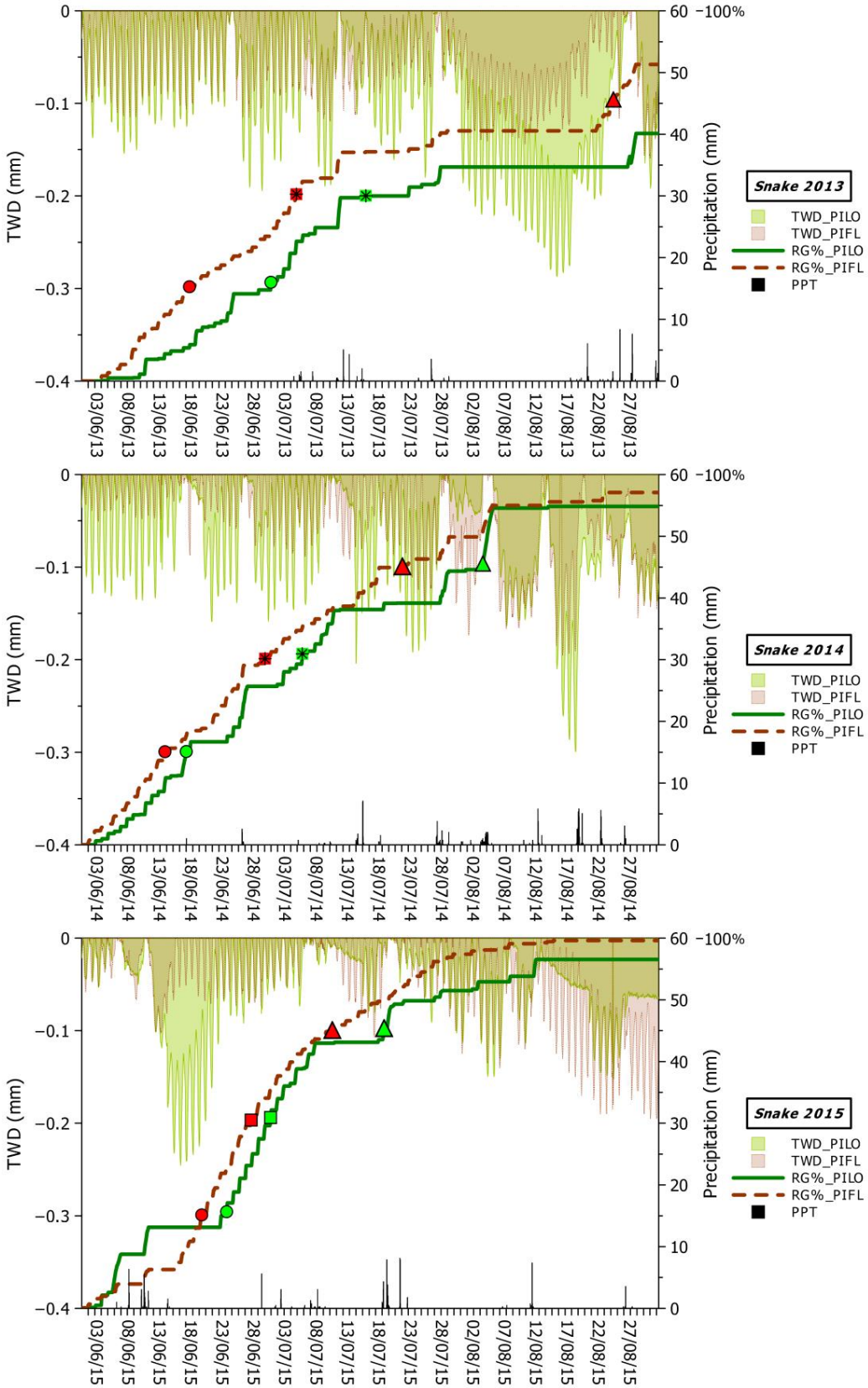

Figure 5. Tree water deficit (TWD) and real growth (RG) time series in 2013–2015 for PILO and PIFL (Snake Range). Symbols represent quartiles of real growth observed between June and September (circles = 25%; squares = 50%; triangles = 75%). Vertical bars represent total hourly precipitation. (Right y axes also represent 100% of RG). For a definition of TWD and RG see main text. Species codes are the same as in the Figure 2 caption.

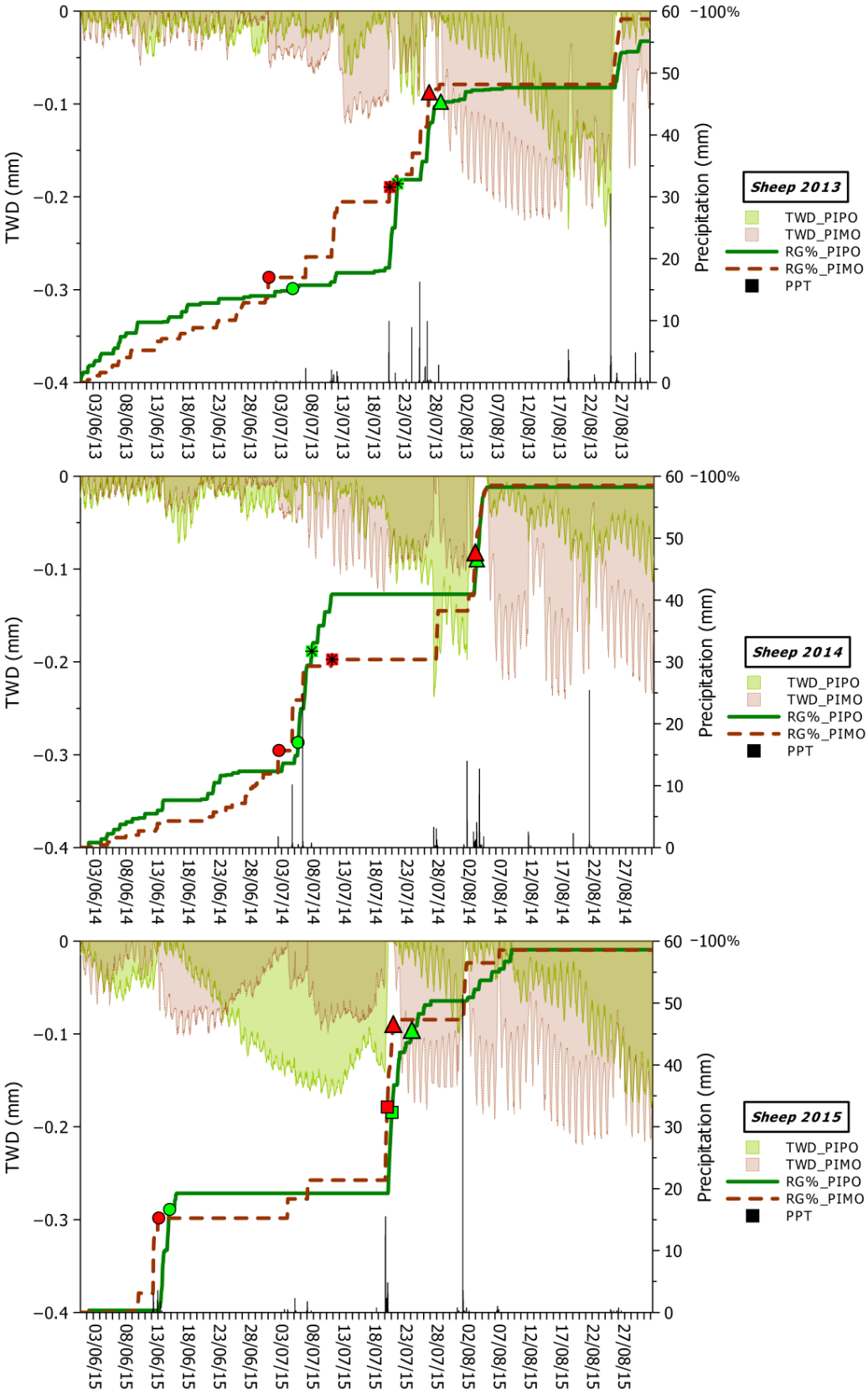

Figure 6. Tree water deficit (TWD) and real growth (RG) time series in 2013–2015 for PIPO and PIMO (Sheep Range). Symbols represent quartiles of real growth observed between June and September (circles = 25%; squares = 50%; triangles = 75%). Vertical bars represent total hourly precipitation. (Right y axes also represent 100% of RG). For a definition of TWD and RG see main text. Species codes are the same as in the Figure 2 caption.

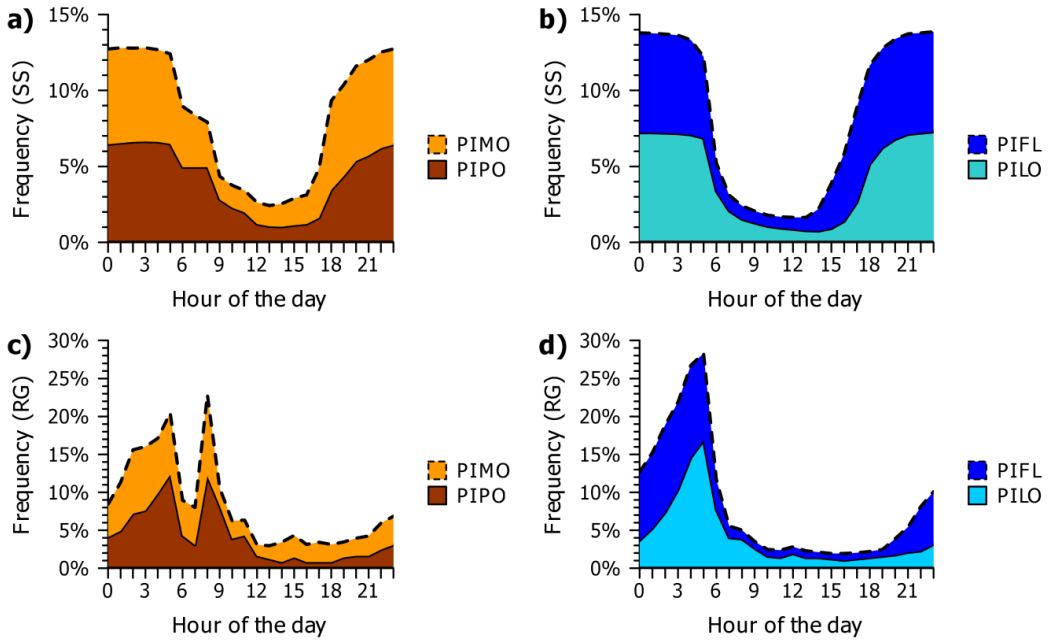

Figure 7. Average daily cycles of stem swelling (SS) and real growth (RG). Graphs (**a**) and (**c**) are for the Sheep Range; graphs (**b**) and (**d**) are for the Snake Range. Species codes are the same as in the Figure 2 caption.

Precipitation was the main predictor of stem swelling (SS) and radial growth (RG), appearing in all logistic models developed for day (Table S1) and night (Table S2) hours, although with different significance. Precipitation increased the odds of stem swelling and radial increment, and species response was less than six hours. During the day, a 1-mm increase in total precipitation in the previous 3 h increased the odds of SS by 2 and 2.5 times in PILO and PIFL respectively. At the Sheep Range, PIPO responded immediately to PPT (lag0), while the odds of SS in PIMO were affected by total precipitation in the previous 6 hours (Table S1). Precipitation in the previous hour was a significant predictor of RG in PIMO during both day- and night-time, and it increased the odds of RG by 1.2 times in PILO as well. Air temperature, vapor pressure deficit, and soil temperature were the other variables that emerged as significant predictors of SS and RG, although at different time lags depending on the species (Table S1). In general, AirT had a negative effect on the probability of SS and RG in all species during the day. At the Snake Range, stem swelling was favored by cooler mean temperatures in the previous hour in PILO and 24 h in PIFL. Within these time frames, a 1-°C increase in air temperature would make stem swelling 0.8 and 0.9 times less likely to happen respectively in PILO and PIFL. During the night, stem swelling was promoted by warm temperatures even at the Sheep Range (Table S2), where AirT in the previous 3 h significantly reduced the odds of RG, respectively 0.8 and 0.6 times in PIPO and PIMO. Vapor pressure deficit negatively affected both SS and RG in all species, but in particular it decreased the odds of irreversible growth during the day at the Snake Range, and the odds of stem swelling during the night at the Sheep Range. Warm soils favored SS at the Snake Range and RG of PIMO at the Sheep Range, despite limited daily variability of soil temperature.

All logistic regressions passed the Hosmer-Lemeshow test at the Sheep Range but not at the Snake Range (Tables S1 and S2). Model performances assessed through the area under the ROC curve varied by species and by process (i.e., stem swelling vs. real growth). At the Snake Range the daily dynamics of stem water replenishment were better captured for PILO, where multiple logistic regression successfully predicted 76.1% of events, while at the Sheep Range daily stem swelling dynamics were less well captured by the models identified for PIPO (65.8%) and PIMO (53.1%) (Table S1 and Figure S2a). During the night, logistic regressions correctly predicted events of SS 65.8% and 55.3% of times in PIPO and PIMO (Table S2 and Figure S2b). Within species and sites, real growth

was in general better modeled than SS, with models for PIMO and PIPO predicting, respectively, 88.9% and 74.1% of RG events during the day (Table S1 and Figure S2c) and 74.9% and 75.8% during the night (Table S2 and Figure S2d). At the Snake Range, irreversible radial increment during the day was successfully predicted 96.2% in PIFL, but less well during the night (79.5% and 56.4% of events captured in PILO and PIFL respectively).

4. Discussion

4.1. Seasonal Dynamics of Circadian Cycles

The mechanisms underlying plant-water relationships and tree hydraulic status have been investigated on a large number of species under controlled conditions, but much less research has focused on understanding how such mechanisms are modulated by environmental and climatic factors in natural conditions [8,9,23]. Albeit not including all co-existing tree species, our two study areas are both representative of natural sky-island forests in the Great Basin and Mojave Deserts [30], and differ remarkably for the seasonal dynamics of total precipitation and soil temperature. Therefore they provide a unique opportunity to investigate daily and seasonal relationships between stem size variations, tree water status, and their environmental drivers. At the subalpine Snake Range site, lower air and soil temperatures together with the seasonal dynamics of the snowpack affect tree growth, especially in the spring and early fall. At the Sheep Range monsoonal rainfall occurring in July and August determines a temporary improvement of water availability, with higher soil and atmospheric moisture, alternating with hyperarid periods. The similar duration of circadian stem cycles at the two locations points toward a strong climatic control over the timing of replenishment (i.e., stem expansion) and depletion (i.e., stem contraction) of tree water reserves (Figure S3). Onset of stem water replenishment is much more variable than the onset of stem contraction in all species, regardless of diurnal or long cycles. This pattern suggests that even if environmental parameters driving transpiration (in particular temperature) play a primary role in stem-water dynamics [11,20,49], replenishment of stem water reserves in these arid environments may start anytime during the day if additional moisture is supplied [50]. The expansion phase began 1–2 h earlier in the afternoon in species characterized by smaller individuals, i.e., PIFL at the Snake Range and PIMO at the Sheep, compared to PILO and PIPO, suggesting that tree size, including stem diameter and crown dimension, could also influence stem rehydration.

The average yearly number of cycles was similar between species, and so was the proportion of long cycles, which ranged between 15 and 20%. The magnitude of both diurnal and long cycles is lower at the Sheep Range, even though the duration of long cycles, especially in PIPO, is greater. This is likely related to the fact that precipitation at the Sheep Range was episodic and concentrated in few abundant rainstorms that greatly raised soil moisture. The temporary improvement of moisture conditions triggered long cycles even though the severe evapotranspiration demands of the Sheep Range limited the magnitude of the radial increment. The importance for PIPO and PIMO of monsoonal water supplied in July and August is evident from the dynamics of stem size variation occurring after minor precipitation events (i.e., <5 mm/day). These atmospheric events are not strong enough to trigger a long cycle, and moderate stem increments associated with the temporary improvement of moisture conditions are usually followed by a sudden stem shrinkage driven by high transpiration related to summer air temperature. Most likely, under hyperarid conditions, once stem water has been refilled, environmental factors controlling transpiration determine whether stem water fulfils transpiration demands or can be diverted to the formation of new xylem cells [51].

Average monthly circadian cycles at the Sheep Range suggest that seasonality of soil freezing/thawing has little effect on stem water dynamics. Since mean soil and air temperature rarely drop below freezing, the risk of frost-induced cavitation for species growing at the southern site is limited if not absent. On the other hand, the reversal of stem cycle phases in winter compared to summer/early fall at the Snake Range indicates that extra-cellular water freezes during the cold season, creating

a withdrawal of water from the bark and the outer stem tissues that leads to frost-induced stem shrinkage, reaching its peak in the coldest hours of the morning [52]. Reversed-phase circadian cycles between winter and summer months are commonly observed in mountain regions [20] but not in species experiencing mild winter temperatures [53].

4.2. Climatic Drivers of Stem Swelling and Real Growth

Cumulative dendrometer series showed that radial increment was more sustained in the northern species compared to the southern ones. More importantly, they captured site- and species-specific strategies to cope with seasonal heat and drought stress, reflecting a high level of phenological plasticity and adaptation to local conditions, in particular at the Sheep Range. PILO and PIFL present a well-defined period of stem enlargement, starting in April–May, continuing as a steep monotonic increase from June to August, and finally reaching a plateau in September. This pattern is typical of conifer species in cold environments [22,54] or from regions characterized by winter dormancy [55,56], and reflects the potential limitations imposed by frozen soil water during the first phases of xylogenesis [57]. At the Sheep Range, stem enlargement is not continuous from June to September but rather episodic, with peaks in radial increment occurring during summer monsoonal rainstorms, as particularly evident in 2015.

Logistic regression models were better at predicting irreversible radial growth than stem swelling (i.e., replenishment of water reserves), especially during daytime. Cellular measurements of wood formation conducted on PIPO at the Sheep Range in 2015 have linked stem rehydration driven by summer precipitation with enhanced cellular division, leading to the rapid formation of new layers of xylem, especially after dry winters, starting in mid-July [43]. These findings align with previous studies from Northern Arizona, where stem radial growth and net photosynthetic rates in PIPO were found to peak in July and August [58], when water stress is relieved by monsoonal precipitation [59]. Studies on wood formation conducted in 2013 and 2014 at the Snake Range on PILO [35] and PIFL [14] have highlighted seasonal patterns of xylem production comparable to radial growth dynamics recorded by point dendrometers, with new cell formation starting in June and ending in late August/early September.

A relatively limited number of variables (i.e., precipitation, air temperature, vapor pressure deficit, and soil temperature) affected stem circadian phenology at both sites. The recurrent presence of precipitation and air temperature as predictors for the presence/absence of stem swelling and irreversible increment suggests that patterns of radial growth reflect site-specific dynamics of evapotranspiration and interactions between moisture conditions and heat. All four pine species experienced prolonged periods of intense water deficit, characterized by no irreversible expansion. During such periods, the recharge of stem water reserves is incomplete, implying that water potential in the cambium remains negative and no radial growth takes place [44]. The range of tree water deficit was similar between sites, but subalpine species in the first part of the growing season presented daily variation of stem size larger than the montane ones. Nevertheless, PILO and PIFL produced regular radial increment, reducing stem water deficit at least for a few hours. PIPO and PIMO showed limited water deficit in June, but then entered a long phase of severe water deficit interrupted only by summer rainstorms.

Climatic response varied by site and species. At the Snake Range, soil temperature emerged as an important driver of stem water replenishment. We then infer that species growing at high elevations, like PILO and PIFL, benefit from increasing soil temperature even in semi-arid environments because in warmer soils water viscosity increases, enhancing root water supply and growth [60], whereas low soil temperature also decreases root hydraulic conductivity by inhibiting aquaporin activity [61]. The shifting sign in the relationship between air temperature and SS (negative during the day, positive at night), is consistent with the high transpiration demands of both sites which largely affect the daily circadian phenology for all species. On the other hand, the effect of air temperature on the odds of irreversible growth seems to be equally fast in both PIPO and PIMO, but much different in PILO and PIFL, with this last species responding to air temperature over a much longer period (12 h).

This finding highlights the role of canopy architecture in controlling transpiration rates, as larger trees with more portions of crown exposed to incoming solar radiation tend to transpire more than smaller ones [62].

All species showed a fast response to total precipitation for time lags up to 6 h, in particular during the day. While the contribution of precipitation to stem swelling was highly significant for all species, PIMO was the only species for which precipitation had an immediate effect (in the previous hour) on irreversible growth. This behavior shows that PIMO is able to use even small amounts of precipitation during the growing season [23], likely due to a combination of higher transpiration demands and lower internal stem water reserves. Large trees can store water in the canopy and in the sapwood [17] to compensate for hydraulic limitations imposed by reduced moisture availability [16]. A species like PIPO can rely on internal reserves of stem water thanks to a particularly high proportion of sapwood [63], while species characterized by smaller trees like PIMO might rely more on water stored in the canopy. Since canopy reserves are rapidly depleted by transpiration [50], species with lower stem water reserves (i.e., sapwood) would then be more dependent on external sources (i.e., precipitation) to replenish them. In this sense, small individuals might be favored against larger ones in a drier/warmer climate [62]. The presence of a negative, yet non-significant, effect of precipitation in the logistic regressions describing RG for PILO and PIFL may suggest that climate-growth relationships near treeline are more complex than at lower elevations [64].

4.3. Implications for Species Adaptation to Climate Change

The fate of tree species under future warming scenarios depends upon their plasticity to adapt, in particular to more frequent and severe droughts [65], hence research on drought-induced tree mortality and its causes is essential to predict future vulnerability of forest species [66,67]. Compensatory mechanisms have been observed via increased water use efficiency [68], physiological short-term regulation [69], or phenological avoidance of dry periods [70]. At the same time, more severe and frequent droughts have been identified as main drivers of reduced tree growth [71,72] and extensive forest die-off, often associated with increased fire frequency and insect outbreaks [73,74]. A trade-off between drought resistance and post-drought recovery has been observed in conifers growing under contrasting climatic conditions, with trees from mesic sites showing higher resistance and trees from xeric conditions showing higher resilience [75]. However, analyses of drought response patterns in relation to stem size variations measured by dendrometers are still scarce in the western US [76].

Conifer species included in our study showed a high level of adaptation to moisture and heat stress, which is reflected in their rapid response to even limited water supplies and to cooler temperatures. The ability of conifer species growing at the xeric southern site to utilize episodic precipitation events during an otherwise hyperarid growing season may represent an adaptation to extremely variable conditions. In particular, it points toward opportunistic growth strategies driven by a high phenological plasticity, which allows xeric southern species to adjust the timing of stem water dynamics with improved moisture conditions (i.e., higher soil water content) and reduced evapotranspiration demands (i.e., lower vapor pressure deficit). The fast response of PIMO to episodic rainfall might explain why single-needle pinyon populations were minimally affected by early 2000s drought episodes, and have continued expanding in the Great Basin [77], whereas Colorado pinyon (*Pinus edulis* Engelm.) has shown unusually high mortality rates in recent decades. Ponderosa pine was previously shown to possess high phenological plasticity [43] and greater capacity to recover pre-drought growth rates in old trees compared to young ones [78], pointing again to the importance of internal stem water reserves for this species.

Rather than on phenological plasticity, adaptability of northern, five-needle species (PILO and PIFL) to a changing climate might depend on the presence of favorable microclimates [79], which determine less demanding evapotranspiration conditions. Rugged montane topography might reduce the effect of climate warming by sheltering temperature-sensitive species [80], and some populations of limber pine in the eastern Sierra Nevada have in fact retreated downslope in cool ravines to escape increasingly dry conditions [81]. High-elevation species like PILO, whose growth dynamics are

tightly linked to snowpack dynamics, might also develop different crown architectures in response to rising temperatures [82]. Bristlecone pine growing under water limitation regimes at the White Mountains maintains erect growth up to the treeline, whereas at the Snake Range krummholz growth forms are more frequent [83]. In general, higher soil moisture, steep slopes, and shallow rocky soils, all conditions found at the Snake Range site, favor strategies of drought resistance rather than post-drought recovery [65], and the sparse structure of such high-elevation stands might actually promote drought adaptation [81].

5. Conclusions

Dendrometer observations provided valuable information about tree responses to environmental stressors. We found that stem circadian phenology of four foundation conifer species growing in sky-island forests on desert mountains in the western USA were controlled directly by moisture or indirectly by those factors favoring accessibility to available water. In warmer and drier habitats, evapotranspiration demands, defined by a combination of air temperature and water availability, were crucial in determining the possibility for conifer species to mitigate tree water deficit and produce irreversible radial growth. In cooler and moister habitats, warm soil temperature was required to facilitate the uptake of soil moisture, derived from a melting snowpack, by subalpine conifers in order to recharge their internal reserves. The different thermal regimes at the Sheep Range (southern site) and at the Snake Range (northern site) resulted in phase-reversed circadian cycles between cold and warm seasons at the northern site but not at the southern one.

Our findings highlighted drought responses that can help understand future tree growth and survival under a changing climate. At the southern site (Sheep Range), conifer species growing in xeric conditions were able to utilize episodic precipitation events during an otherwise hyperarid growing season. Such pattern was not present in near-treeline five-needle pines from the northern site (Snake Range), where seasonal dynamics of stem radial phenology were linked to spring conditions and their linkages to moisture provided by snowpack melting.

Supplementary Materials: The following are available online at http://www.mdpi.com/1999-4907/9/7/396/s1, Figure S1: Relationships between duration and magnitude of circadian phases; Figure S2: Discrimination capacity of logistic regression for SS and RG; Figure S3: Stem-cycle phases of contraction, expansion, and increment for the Snake Range and the Sheep Range; Table S1: Statistics for logistic regression models for day hours; Table S2: Statistics for logistic regression models for night hours.

Author Contributions: Conceptualization, F.B. and E.Z.; Methodology, E.Z. and F.B.; Formal Analysis, E.Z.; Writing-Original Draft Preparation, E.Z.; Writing-Review & Editing, F.B.; Visualization, E.Z.; Supervision, F.B.; Project Administration, F.B.; Funding Acquisition, F.B.

Funding: This research was funded, in part, by the US National Science Foundation under grants AGS-P2C2-1401381 to F. Biondi and AGS-P2C2-1502379 to F. Biondi and E. Ziaco. Additional funding was provided to F. Biondi by the Office of the Vice President for Research and Innovation at the University of Nevada, Reno, in relation to NevCAN. The views and conclusions contained in this document are those of the authors and should not be interpreted as representing the opinions or policies of the funding agencies and supporting institutions.

Acknowledgments: We thank S. Strachan for NevCAN maintenance, R. Hill for compiling dendrometer data, E. van der Maaten and M. van der Maaten-Theunissen for helpful discussion of the R package dendrometeR.

Conflicts of Interest: The authors declare no conflict of interest. The funders had no role in the design of the study; in the collection, analyses, or interpretation of data; in the writing of the manuscript, and in the decision to publish the results.

References

1. Mendivelso, H.A.; Camarero, J.J.; Gutiérrez, E.; Zuidema, P.A. Time-dependent effects of climate and drought on tree growth in a Neotropical dry forest: Short-term tolerance vs. long-term sensitivity. *Agr. Forest Meteorol.* **2014**, *188*, 13–23. [CrossRef]
2. George, S.S. An overview of tree-ring width records across the Northern Hemisphere. *Quat. Sci. Rev.* **2014**, *95*, 132–150. [CrossRef]

3. Kocher, P.; Horna, V.; Leuschner, C. Environmental control of daily stem growth patterns in five temperate broad-leaved tree species. *Tree Physiol.* **2012**, *32*, 1021–1032. [CrossRef] [PubMed]
4. Deslauriers, A.; Anfodillo, T.; Rossi, S.; Carraro, V. Using simple causal modeling to understand how water and temperature affect daily stem radial variation in trees. *Tree Physiol.* **2007**, *27*, 1125–1136. [CrossRef] [PubMed]
5. Sevanto, S.; McDowell, N.G.; Dickman, L.T.; Pangle, R.; Pockman, W.T. How do trees die? A test of the hydraulic failure and carbon starvation hypotheses. *Plant Cell Environ.* **2014**, *37*, 153–161. [CrossRef] [PubMed]
6. Steppe, K.; Sterck, F.; Deslauriers, A. Diel growth dynamics in tree stems: Linking anatomy and ecophysiology. *Trends Plant Sci.* **2015**, *20*, 335–343. [CrossRef] [PubMed]
7. Coussement, J.R.; De Swaef, T.; Lootens, P.; Roldán-Ruiz, I.; Steppe, K. Introducing turgor-driven growth dynamics into functional-structural plant models. *Ann. Bot.* **2018**, *121*, 849–861. [CrossRef] [PubMed]
8. van der Maaten, E.; Bouriaud, O.; van der Maaten-Theunissen, M.; Mayer, H.; Spiecker, H. Meteorological forcing of day-to-day stem radius variations of beech is highly synchronic on opposing aspects of a valley. *Agr. Forest Meteorol.* **2013**, *181*, 85–93. [CrossRef]
9. Oberhuber, W. Soil water availability and evaporative demand affect seasonal growth dynamics and use of stored water in co-occurring saplings and mature conifers under drought. *Trees-Struct. Funct.* **2017**, *31*, 467–478. [CrossRef] [PubMed]
10. De Swaef, T.; De Schepper, V.; Vandegehuchte, M.W.; Steppe, K. Stem diameter variations as a versatile research tool in ecophysiology. *Tree Physiol.* **2015**, *35*, 1047–1061. [CrossRef] [PubMed]
11. Herzog, K.M.; Häsler, R.; Thum, R. Diurnal changes in the radius of a subalpine Norway spruce stem: their relation to the sap flow and their use to estimate transpiration. *Trees* **1995**, *10*, 94–101. [CrossRef]
12. Zweifel, R.; Item, H.; Hasler, R. Link between diurnal stem radius changes and tree water relations. *Tree Physiol.* **2001**, *21*, 869–877. [CrossRef] [PubMed]
13. Braekke, F.H.; Kozlowski, T.T. Shrinkage and swelling of stems of Pinus resinosa and Betula papyrifera in northern Wisconsin. *Plant Soil* **1975**, *43*, 387–410. [CrossRef]
14. Ziaco, E.; Biondi, F. Tree growth, cambial phenology, and wood anatomy of limber pine at a Great Basin (USA) mountain observatory. *Trees-Struct. Funct.* **2016**, *30*, 1507–1521. [CrossRef]
15. Zweifel, R.; Haeni, M.; Buchmann, N.; Eugster, W. Are trees able to grow in periods of stem shrinkage? *New Phytol.* **2016**, *211*, 839–849. [CrossRef] [PubMed]
16. Phillips, N.G.; Ryan, M.G.; Bond, B.J.; McDowell, N.G.; Hinckley, T.M.; Čermák, J. Reliance on stored water increases with tree size in three species in the Pacific Northwest. *Tree Physiol.* **2003**, *23*, 237–245. [CrossRef] [PubMed]
17. Čermák, J.; Kučera, J.; Bauerle, W.L.; Phillips, N.; Hinckley, T.M. Tree water storage and its diurnal dynamics related to sap flow and changes in stem volume in old-growth Douglas-fir trees. *Tree Physiol.* **2007**, *27*, 181–198. [CrossRef] [PubMed]
18. Barnard, D.M.; Meinzer, F.C.; Lachenbruch, B.; McCulloh, K.A.; Johnson, D.M.; Woodruff, D.R. Climate-related trends in sapwood biophysical properties in two conifers: avoidance of hydraulic dysfunction through coordinated adjustments in xylem efficiency, safety and capacitance. *Plant Cell Environ.* **2011**, *34*, 643–654. [CrossRef] [PubMed]
19. Meinzer, F.C.; Bond, B.J.; Warren, J.M.; Woodruff, D.R. Does water transport scale universally with tree size? *Funct. Ecol.* **2005**, *19*, 558–565. [CrossRef]
20. King, G.; Fonti, P.; Nievergelt, D.; Büntgen, U.; Frank, D. Climatic drivers of hourly to yearly tree radius variations along a 6 °C natural warming gradient. *Agr. Forest Meteorol.* **2013**, *168*, 36–46. [CrossRef]
21. Turcotte, A.; Rossi, S.; Deslauriers, A.; Krause, C.; Morin, H. Dynamics of depletion and replenishment of water storage in stem and roots of black spruce measured by dendrometers. *Front. Plant Sci.* **2011**, *2*, 21. [CrossRef] [PubMed]
22. Deslauriers, A.; Morin, H.; Urbinati, C.; Carrer, M. Daily weather response of balsam fir (Abies balsamea (L.) Mill.) stem radius increment from dendrometer analysis in the boreal forests of Québec (Canada). *Trees* **2003**, *17*, 477–484. [CrossRef]
23. Biondi, F.; Rossi, S. Plant-water relationships in the Great Basin Desert of North America derived from Pinus monophylla hourly dendrometer records. *Int. J. Biometeorol.* **2015**, *59*, 939–953. [CrossRef] [PubMed]
24. Drew, D.M.; Downes, G.M. The use of precision dendrometers in research on daily stem size and wood property variation: A review. *Dendrochronologia* **2009**, *27*, 159–172. [CrossRef]

25. Grayson, D.K. *The Great Basin: A Natural Prehistory, Revised and Expanded Edition*; University of California Press: Berkeley, CA, USA, 2011.
26. Osmond, C.B.; Pitelka, L.F.; Hidy, G.M. *Plant Biology of the Basin and Range*; Springer-Verlag: Berlin, Germany, 1990; p. 375.
27. Adams, D.K.; Comrie, A.C. The North American Monsoon. *Bull. Am. Meteorol. Soc.* **1997**, *78*, 2197–2213. [CrossRef]
28. Szejner, P.; Wright, W.E.; Babst, F.; Belmecheri, S.; Trouet, V.; Leavitt, S.W.; Ehleringer, J.R.; Monson, R.K. Latitudinal gradients in tree ring stable carbon and oxygen isotopes reveal differential climate influences of the North American Monsoon System. *J. Geophys. Res. Biogeosci.* **2016**, *121*, 1978–1991. [CrossRef]
29. Ellison, A.M.; Bank, M.S.; Clinton, B.D.; Colburn, E.A.; Elliott, K.; Ford, C.R.; Foster, D.R.; Kloeppel, B.D.; Knoepp, J.D.; Lovett, G.M.; et al. Loss of foundation species: Consequences for the structure and dynamics of forested ecosystems. *Front. Ecol. the Environ.* **2005**, *3*, 479–486. [CrossRef]
30. Mensing, S.; Strachan, S.; Arnone, J.; Fenstermaker, L.; Biondi, F.; Devitt, D.; Johnson, B.; Bird, B.; Fritzinger, E. A network for observing Great Basin climate change. *EOS Trans. Amer. Geophys. Union* **2013**, *94*, 105–106. [CrossRef]
31. Johnson, B.G.; Verburg, P.S.J.; Arnone, J.A. Effects of climate and vegetation on soil nutrients and chemistry in the Great Basin studied along a latitudinal-elevational climate gradient. *Plant Soil* **2014**, *382*, 151–163. [CrossRef]
32. Gochis, D.; Schemm, J.; Shi, W.; Long, L.; Higgins, W.; Douglas, A. A Forum for Evaluating Forecasts of the North American Monsoon. *Eos Trans. Amer. Geophys. Union* **2009**, *90*, 249–251. [CrossRef]
33. Biondi, F.; Hartsough, P.C.; Estrada, I.G. Daily weather and tree growth at the tropical treeline of North America. *Arct. Antarctic Alp. Res.* **2005**, *37*, 16–24. [CrossRef]
34. Biondi, F.; Hartsough, P. Using automated point dendrometers to analyze tropical treeline stem growth at Nevado de Colima, Mexico. *Sensors* **2010**, *10*, 5827. [CrossRef] [PubMed]
35. Ziaco, E.; Biondi, F.; Rossi, S.; Deslauriers, A. Environmental drivers of cambial phenology in Great Basin bristlecone pine. *Tree Physiol.* **2016**, *36*, 818–831. [CrossRef] [PubMed]
36. Lawrence, M.G. The Relationship between Relative Humidity and the Dewpoint Temperature in Moist Air: A Simple Conversion and Applications. *Bull. Amer. Meteorol. Soc.* **2005**, *86*, 225–233. [CrossRef]
37. Feld, S.I.; Cristea, N.C.; Lundquist, J.D. Representing atmospheric moisture content along mountain slopes: Examination using distributed sensors in the Sierra Nevada, California. *Water Resour. Res.* **2013**, *49*, 4424–4441. [CrossRef]
38. McEvoy, D.J.; Mejia, J.F.; Huntington, J.L. Use of an Observation Network in the Great Basin to Evaluate Gridded Climate Data. *J. Hydrometeorol.* **2014**, *15*, 1913–1931. [CrossRef]
39. Kunkel, K.E. Simple procedures for extrapolation of humidity variables in the mountainous western United States. *J. Clim.* **1989**, *2*, 656–669. [CrossRef]
40. Maaten, E.V.D.; Maaten-Theunissen, M.V.D.; Smiljanić, M.; Rossi, S.; Simard, S.; Wilmking, M.; Deslauriersb, A.; Fontie, P.; Arxe, G.; Bouriaudf, O. DendrometeR: Analyzing the pulse of trees in R. *Dendrochronologia* **2016**, *40*, 12–16. [CrossRef]
41. R Core Team. R: A Language and Environment for Statistical Computing. R Foundation for Statistical Computing: Vienna, Austria, 2015.
42. Deslauriers, A.; Rossi, S.; Turcotte, A.; Morin, H.; Krause, C. A three-step procedure in SAS to analyze the time series from automatic dendrometers. *Dendrochronologia* **2011**, *29*, 151–161. [CrossRef]
43. Ziaco, E.; Truettner, C.; Biondi, F.; Bullock, S. Moisture-driven xylogenesis in Pinus ponderosa from a Mojave Desert mountain reveals high phenological plasticity. *Plant Cell Environ.* **2018**, *41*, 823–836. [CrossRef] [PubMed]
44. Chan, T.; Berninger, F.; Mencuccini, M.; Nikinmaa, E. Separating water-potential induced swelling and shrinking from measured radial stem variations reveals a cambial growth and osmotic concentration signal. *Plant Cell Environ.* **2016**, *39*, 233–244. [CrossRef] [PubMed]
45. Hosmer, J.D.W.; Lemeshow, S.; Sturdivant, R.X. *The Multiple Logistic Regression Model, in Applied Logistic Regression*; John Wiley & Sons: Hoboken, NJ, USA, 2013; pp. 35–47.
46. Quinn, G.P.; Keough, M.J. *Experimental Design and Data Analysis for Biologists*; Cambridge University Press: Cambridge, UK, 2002.

47. Pearce, J.; Ferrier, S. Evaluating the predictive performance of habitat models developed using logistic regression. *Ecol. Modell.* **2000**, *133*, 225–245. [CrossRef]
48. Robin, X.; Turck, N.; Hainard, A.; Tiberti, N.; Lisacek, F.; Sanchez, J.C.; Müller, M. pROC: an open-source package for R and S+ to analyze and compare ROC curves. *BMC Bioinformatics* **2011**, *12*, 77. [CrossRef] [PubMed]
49. Oberhuber, W.; Hammerle, A.; Kofler, W. Tree water status and growth of saplings and mature Norway spruce (Picea abies) at a dry distribution limit. *Front. Plant Sci.* **2015**, *6*, 703. [CrossRef] [PubMed]
50. Zweifel, R.; Häsler, R. Dynamics of water storage in mature subalpine Picea abies: Temporal and spatial patterns of change in stem radius. *Tree Physiol.* **2001**, *21*, 561–569. [CrossRef] [PubMed]
51. Maherali, H.; DeLucia, E.H. Influence of climate-driven shifts in biomass allocation on water transport and storage in ponderosa pine. *Oecologia* **2001**, *129*, 481–491. [CrossRef] [PubMed]
52. Zweifel, R.; Häsler, R. Frost-induced reversible shrinkage of bark of mature subalpine conifers. *Agr. Forest Meteorol.* **2000**, *102*, 213–222. [CrossRef]
53. Vieira, J.; Rossi, S.; Campelo, F.; Freitas, H.; Nabais, C. Seasonal and daily cycles of stem radial variation of Pinus pinaster in a drought-prone environment. *Agr. Forest Meteorol.* **2013**, *180*, 173–181. [CrossRef]
54. Tardif, J.; Flannigan, M.; Bergeron, Y. An Analysis of the Daily Radial Activity of 7 Boreal Tree Species, Northwestern Quebec. *Environ. Monit. Assess.* **2001**, *67*, 141–160. [CrossRef] [PubMed]
55. Güney, A.; Küppers, M.; Rathgeber, C.; Şahin, M.; Zimmermann, R. Intra-annual stem growth dynamics of Lebanon Cedar along climatic gradients. *Trees* **2017**, *31*, 1–20. [CrossRef]
56. Linares, J.C.; Camarero, J.J.; Carreira, J.A. Plastic responses of Abies pinsapo xylogenesis to drought and competition. *Tree Physiol.* **2009**, *29*, 1525–1536. [CrossRef] [PubMed]
57. Rossi, S.; Morin, H.; Deslauriers, A. Multi-scale influence of snowmelt on xylogenesis of black spruce. *Arct. Antarct. Alp. Res.* **2011**, *43*, 457–464. [CrossRef]
58. Gaylord, M.L.G.L.; Kolb, T.E.K.E.; Wallin, K.F.W.F.; Wagner, M.R.W.R. Seasonal dynamics of tree growth, physiology, and resin defenses in a northern Arizona ponderosa pine forest. *Can. J. Forest Res.* **2007**, *37*, 1173–1183. [CrossRef]
59. Kolb, T.E.; Stone, J.E. Differences in leaf gas exchange and water relations among species and tree sizes in an Arizona pine-oak forest. *Tree Physiol.* **2000**, *20*, 1–12. [CrossRef] [PubMed]
60. Kozlowski, T.T. Soil moisture and absorption of water by tree roots. *J. Arboric.* **1987**, *13*, 39–46.
61. Gambetta, G.A.; Knipfer, T.; Fricke, W.; Mcelrone, A.J. Aquaporins and Root Water Uptake. In *Plant Aquaporins: From Transport to Signaling*; Chaumont, F., Tyerman, S.D., Eds.; Springer International Publishing: New York, NY, USA, 2017; pp. 133–153.
62. Bennett, A.C.; Mcdowell, N.G.; Allen, C.D.; Andersonteixeira, K.J. Larger trees suffer most during drought in forests worldwide. *Nat. Plants* **2015**, *1*, 15139. [CrossRef] [PubMed]
63. Domec, J.C.; Gartner, B.L. Relationship between growth rates and xylem hydraulic characteristics in young, mature and old-growth ponderosa pine trees. *Plant Cell Environ.* **2003**, *26*, 471–483. [CrossRef]
64. Hughes, M.K.; Funkhouser, G. Frequency-Dependent Climate Signal in Upper and Lower Forest Border Tree Rings in the Mountains of the Great Basin. *Clim. Change* **2003**, *59*, 233–244. [CrossRef]
65. Gazol, A.; Camarero, J.J.; Anderegg, W.R.L.; Vicente-Serrano, S.M. Impacts of droughts on the growth resilience of Northern Hemisphere forests. *Global Ecol. Biogeogr.* **2017**, *26*, 166–176. [CrossRef]
66. Allen, C.D.; Breshears, D.D.; McDowell, N.G. On underestimation of global vulnerability to tree mortality and forest die-off from hotter drought in the Anthropocene. *Ecosphere* **2015**, *6*, art129. [CrossRef]
67. Grossiord, C.; Sevanto, S.; Borrego, I.; Chan, A.M.; Collins, A.D.; Dickman, L.T.; Hudson, P.J.; McBranch, N.; Michaletz, S.T.; Pockman, W.T.; et al. Tree water dynamics in a drying and warming world. *Plant Cell Environ.* **2017**, *40*, 1861–1873. [CrossRef] [PubMed]
68. Peñuelas, J.; Canadell, J.G.; Ogaya, R. Increased water-use efficiency during the 20th century did not translate into enhanced tree growth. *Global Ecol. Biogeogr.* **2011**, *20*, 597–608. [CrossRef]
69. Mencuccini, M. The ecological significance of long-distance water transport: short-term regulation, long-term acclimation and the hydraulic costs of stature across plant life forms. *Plant Cell Environ.* **2003**, *26*, 163–182. [CrossRef]
70. Limousin, J.M.; Rambal, S.; Ourcival, J.M.; Rodríguezcalcerrada, J.; Pérezramos, I.M.; Rodríguezcortina, R.; Misson, L.; Joffre, R. Morphological and phenological shoot plasticity in a Mediterranean evergreen oak facing long-term increased drought. *Oecologia* **2012**, *169*, 565–577. [CrossRef] [PubMed]

71. Griffin, D.; Anchukaitis, K.J. How unusual is the 2012–2014 California drought? *Geophys. Res. Lett.* **2014**, *41*, 9017–9023. [CrossRef]
72. Anderegg, W.R.; Schwalm, C.; Biondi, F.; Camarero, J.J.; Koch, G.; Litvak, M.; Ogle, K.; Shaw, J.D.; Shevliakova, E.; Williams, P.; et al. Pervasive drought legacies in forest ecosystems and their implications for carbon cycle models. *Science* **2015**, *349*, 528–532. [CrossRef] [PubMed]
73. Anderegg, W.R.L.; Kane, J.M.; Anderegg, L.D.L. Consequences of widespread tree mortality triggered by drought and temperature stress. *Nat. Clim. Change* **2013**, *3*, 30–36. [CrossRef]
74. Williams, A.P.; Allen, C.D.; Macalady, A.K.; Griffin, D.; Woodhouse, C.A.; Meko, D.M.; Swetnam, T.W.; Rauscher, S.A.; Seager, R.; Grissino-Mayer, H.D.; et al. Temperature as a potent driver of regional forest drought stress and tree mortality. *Nat. Clim. Change* **2012**, *3*, 292. [CrossRef]
75. Sánchez-Salguero, R.; Camarero, J.J.; Rozas, V.; Génova, M.; Olano, J.M.; Arzac, A.; Gazol, A.; Caminero, L.; Tejedor, E.; Luis, M.; et al. Resist, recover or both? Growth plasticity in response to drought is geographically structured and linked to intraspecific variability in Pinus pinaster. *J. Biogeogr.* **2018**, *45*, 1–14. [CrossRef]
76. Martin, J.; Looker, N.; Hoylman, Z.; Jencso, K.; Hu, J. Hydrometeorology organizes intra-annual patterns of tree growth across time, space and species in a montane watershed. *New Phytol.* **2017**, *215*, 1387–1398. [CrossRef] [PubMed]
77. Biondi, F.; Bradley, M.L. Long-term survivorship of single-needle pinyon (Pinus monophylla) in mixed-conifer ecosystems of the Great Basin, USA. *Ecosphere* **2013**, *4*, art120. [CrossRef]
78. Lloret, F.; Keeling, E.G.; Sala, A. Components of tree resilience: effects of successive low-growth episodes in old ponderosa pine forests. *Oikos* **2011**, *120*, 1909–1920. [CrossRef]
79. Daly, C.; Conklin, D.R.; Unsworth, M.H. Local atmospheric decoupling in complex topography alters climate change impacts. *Int. J. Climatol.* **2010**, *30*, 1857–1864. [CrossRef]
80. Loarie, S.R.; Duffy, P.B.; Hamilton, H.; Asner, G.P.; Field, C.B.; Ackerly, D.D. The velocity of climate change. *Nature* **2009**, *462*, 1052. [CrossRef] [PubMed]
81. Millar, C.I.; Westfall, R.D.; Delany, D.L. Response of high-elevation limber pine (Pinus flexilis) to multiyear droughts and 20th-century warming, Sierra Nevada, California, USA. *Can. J. Forest Res.* **2007**, *37*, 2508–2520. [CrossRef]
82. Millar, C.I.; Westfall, R.D.; Delany, D.L.; King, J.C.; Graumlich, L.J. Response of Subalpine Conifers in the Sierra Nevada, California, U.S.A., to 20th-Century Warming and Decadal Climate Variability. *Arc. Antarct. Alp. Res.* **2004**, *36*, 181–200. [CrossRef]
83. LaMarche, V.C., Jr.; Mooney, H.A. Recent climatic change and development of the bristlecone pine (P. longaeva Bailey) krummholz zone, Mt. Washington Nevada. *Arc. Alp. Res.* **1972**, *4*, 61–72. [CrossRef]